Tropospheric Corrections for Coastal Altimetry

6

E. Obligis, C. Desportes, L. Eymard, M.J. Fernandes, C. Lázaro, and A.L. Nunes

Contents

Keywords Altimetry • GPS • Microwave radiometry • Water vapor • Wet tropospheric correction

E. Obligis (✉)
Collecte Localisation Satellites, 8-10 rue Hermes, 31520, Ramonville St-Agne, France

C. Desportes
Mercator Ocean, 8-10 rue Hermès, 31520 Ramonville, St Agne, France

L. Eymard
IPSL/LOCEAN, Université Pierre et Marie Curie, 4 Place Jussieu, 75252, Paris, France

M.J. Fernandes and C. Lázaro
Faculdade de Ciências da Universidade do Porto, Departamento de Matemática Aplicada,
Rua do Campo Alegre, 687, 4169-007, Porto, Portugal

A.L. Nunes
Instituto Superior de Engenharia do Porto, Rua Dr. António Bernardino de Almeida, 431,
4200-072, Porto, Portugal

Abbreviations

2T	2-meter Temperature
COASTALT	ESA development of COASTal ALTimetry
CorSSH	corrected Sea Surface Height
dB	Decibel
DLM	Dynamically Linked Model
ECMWF	European Centre for Medium-Range Weather Forecasts
EPN	EUREF Permanent Network
ESA	European Space Agency
GDR	Geophysical Data Record
GFO	Geosat Follow-On
GMF	Global Mapping Functions
GNSS	Global Navigation Satellite System
GPD	GNSS-derived Path Delay
GPS	Global Positioning System
IGS	International GNSS Service
MWR	Microwave Radiometer
NCEP	U.S. National Centers for Environmental Prediction
NWM	Numerical Weather Model
PD	Path Delay
SSM/I	Special Sensor Microwave Imager
STD	Slant Total Delay
T/P	TOPEX/Poseidon
TB	Brightness Temperature
TCWV	Total Column Water Vapour
TMR	TOPEX Microwave Radiometer
VMF1	Vienna Mapping Functions 1
ZHD	Zenith Hydrostatic Delays
ZWD	Zenith Wet Delays

6.1
Introduction

The exploitation of altimetric measurements over ocean relies on the capability to correct the altimeter range from all external perturbations. Two of them are related to the troposphere characteristics and should be estimated to properly correct the altimeter range: the wet and the dry path delays.

The wet tropospheric path delay is almost proportional to the integrated water vapor content of the atmosphere, and strongly affects the range measured by the altimeter. It varies between 0 and 50 cm but with a high variability in space and time. Up to now, meteorological models do not satisfactorily describe water vapour variations (pattern location and extension, magnitude, time evolution, etc…), so a dedicated instrument is added to the mission, a microwave radiometer. However, the radiometer footprint size is much larger than the altimeter one (about

25 km and 5 km for the radiometer and the altimeter, respectively). In open ocean, the combination altimeter/radiometer is satisfactory both in terms of accuracy and spatial resolution, because of the mean scale of major meteorological events (from a few tens of kilometers to several hundreds of kilometers). This is not the case for transition areas (sea/land), because of the radiometer measurement specificities: the given footprint is the 3 dB diameter, meaning that roughly half the signal is coming from outside this footprint. Consequently, the signal coming from the surrounding land surfaces (with a strong and highly time-varying emissivity compared to ocean) contaminates the measurement and makes the humidity retrieval method unsuitable. Furthermore, the spatial and temporal resolutions of meteorological models are not sufficient enough to handle the specific problem related to coastal atmospheric variability: surface temperature gradients between land and sea or relief, for example, may generate specific small-scale atmospheric features that could not be represented in the current model products. This means that, today, for example, Envisat and Jason-1 altimeter measurements located at less than about 50 km from land cannot benefit from a suitable correction.

Nevertheless, the exploitation of altimeter measurements in coastal areas becomes a challenge for oceanography. Different dedicated studies have been conducted recently and promising methods are identified today to propose a wet tropospheric correction in these transition areas, which could fulfil the constraint related to altimeter measurement processing, in terms of both accuracy and spatial resolution. Two different strategies have been considered to handle the problem specific to the wet tropospheric correction for coastal altimetry.

The first one, explained in Sect. 6.2, consists of combining information in the coastal area to update and improve the radiometer wet tropospheric correction in the coastal band. We present two different methodologies based on the combination of available information: the dynamically linked model (DLM) approach, based on the dynamic combination of radiometer and model data, and the GNSS-derived Path Delay (GPD) method, based on GNSS (Global Navigation Satellite System)-derived path delays combined with radiometer valid measurements and model-based information.

The second one, presented in Sect. 6.3, consists of the correction of the measured brightness temperatures in order to remove the contamination coming from the surrounding land. An accurate correction allows for the subsequent application of a standard ocean algorithm.

The dry tropospheric path delay is proportional to the sea level pressure and is by far the largest correction to be applied to the altimeter range (higher than 2 m). However, its main characteristic is that its time-variable part is low (lower than 5 mm), so it is quite well estimated using meteorological models. In Sect. 6.4, the main issues related to the computation of the dry correction for open ocean are reviewed. For coastal areas, a first assessment of the accuracy of ECMWF (European Centre for Medium-Range Weather Forecasts)-derived dry tropospheric path delay is presented.

6.2
Combination and Processing of Available Information

In order to improve the computation of the wet tropospheric correction in coastal areas, two methods making use of data other than the microwave radiometer measurements have been developed and are described here. The first one only requires numerical weather model

(NWM) data and radiometer wet tropospheric corrections available on the Geophysical Data Record (GDR) product and has the advantage of being mission-independent. The second approach combines information from tropospheric path delays determined at a network of GNSS stations, valid radiometer measurements and NWM-based information.

6.2.1
Dynamically Linked Model Approach

This section describes the dynamically linked model (DLM) approach, which consists of replacing, in coastal regions, the microwave radiometer (MWR) derived correction with a large-scale atmospheric reanalysis model-derived correction, such as ECMWF, dynamically linked to the closest points with valid MWR correction.

It should be emphasized that this approach is significantly different from the use of the ECMWF model correction everywhere. It is well-known that the wet tropospheric models are not suitable for processing long time series of satellite altimetry since they possess long-term errors and discontinuities (Scharroo et al. 2004). In addition, they possess small-scale errors, which may be due to mislocation and absence of some atmospheric features. Although this method does not compensate for the small-scale errors, it significantly reduces the large-scale ones. This happens because the large-scale errors for small regions, such as land-contaminated tracks in coastal zones, are quasi-linear and will be removed by locally adjusting the NWM to the MWR correction.

The method only requires information available on the GDR – optionally, information from a distance-to-land global grid – and can be implemented globally for any satellite. The question is then which particular strategy should be adopted to ensure the continuity in the transition between the MWR and NWM wet tropospheric correction fields.

The definition of the coastal track segments to be corrected can be based on the microwave radiometer land flag, provided this is reliable. Comparisons with GNSS-derived tropospheric delays show that in some close-to-land regions, at distances less than 30 km from the coastline, the MWR correction can be quite noisy, while the corresponding land MWR flag is still off. This problem can be overcome by using distance-to-land information and ensuring that all points with a distance-to-land smaller than a specified value, e.g., 20 km, are also considered contaminated points and must be corrected. The first approach has the advantage that it only requires information present on the GDR (MWR and NWM corrections and the land MWR flag). The second approach depends on the quality of the coastline used to compute the distance-to-land grid and reduces the possibility that land-contaminated points are left uncorrected, but might lead to the unnecessary correction of valid radiometer points.

Considering a simple but efficient implementation, two types of algorithms can be adopted: an island type and a continental coastline type. The first case is suggested by the land contaminated segments formed around relatively small islands or peninsulas, where a land contaminated segment is formed and there are valid microwave radiometer points on each side of the segment. The second case occurs around the continental coastlines, typically when a satellite is approaching or receding from a large land mass. In this case, there is only a valid MWR correction on one of the sides of the contaminated segment.

In the island type of algorithm, the NWM field is adjusted to the MWR field at the beginning and end of the land contaminated segment by using a linear adjustment. The NWM correction is then dynamically linked to the MWR field at the beginning and end of

the segment, for example, at the first (A) and last (B) points with valid MWR correction. For all contaminated points between A and B, the final field will be equal to the NWM field plus a linear correction, ensuring that at both A and B the microwave radiometer and adjusted numerical weather model fields are the same, achieving the required continuity.

In the continental coastline type of algorithm, there is only valid information on one side of the contaminated segment and therefore it is not possible to perform an adjustment of the NWM and MWR fields by using a linear adjustment. In this case, the adjustment is performed only at the beginning or end of the segment by using a bias correction computed as the difference between the microwave radiometer and numerical weather model fields at the first (A) or last (B) point with valid MWR field. For all contaminated points between the beginning of the segment and A (or between B and the end of the segment), the final field will be equal to the NWM field plus a bias correction, ensuring that at A or B both fields will be the same and therefore continuous.

Prior to this implementation, GDR data shall be separated into segments where a new segment is considered whenever a data gap greater than a specified value, e.g., 20 s, exists. The algorithm shall then be applied to each data segment. In this way, the only points that will not be recovered are segments for which there are no valid microwave radiometer points close enough to perform the adjustment.

Studies conducted by Fernandes et al. (2003) show that this simple approach leads to a data recovery of 80–90% of the invalid measurements in the coastal regions, does not introduce discontinuities in the correction and can be used to generate coastal products in an operational processing scheme. Mercier (2004) has also applied a similar type of algorithm to improve data recovery near the coast.

Fig. 6.1 illustrates two examples of the application of this algorithm to two regions: a continental coastline and a mixed region. In the map on the right-hand side of the figure, the blue points represent land-contaminated points in the microwave radiometer wet tropospheric correction that must be adjusted by the algorithm. In the graphs on the left, the cyan points represent the ECMWF model correction, the red points the original MWR correction and the blue points the final correction after applying the DLM algorithm. In the coastal regions, the original noisy MWR correction (in red) is replaced by the continuous smoother correction (in blue). The green dots represent the algorithm flag: 2 for points which were contaminated and ended corrected, 1 for points which were contaminated but were not corrected and 0 for points that were not contaminated originally.

The performance of the method is directly related to the accuracy of the adopted NWM. Usually, the GDRs provide the wet tropospheric correction from two models: ECMWF and NCEP (U.S. National Centers for Environmental Prediction).

To inspect the differences between the wet tropospheric correction from the onboard microwave radiometer and from the ECMWF and NCEP models, these have been compared with Envisat cycles 48 to 75, corresponding to the period June 2006 to January 2009. Considering only points with valid MWR measurement, covering the whole world, the difference between the MWR and ECMWF corrections is 2 ± 18 mm, while the corresponding difference between the MWR and NCEP is 7 ± 33 mm.

To evaluate the sensitivity of the DLM output to the adopted NWM, the algorithm has been applied to the above-mentioned 28 Envisat cycles, to the whole range of latitudes and longitudes, using each of the above mentioned NWM. A total number of 1,062,058 coastal "land contaminated points" have been corrected (representing 94% of the total number of land contaminated points). For these points, the difference, which before adjustment was
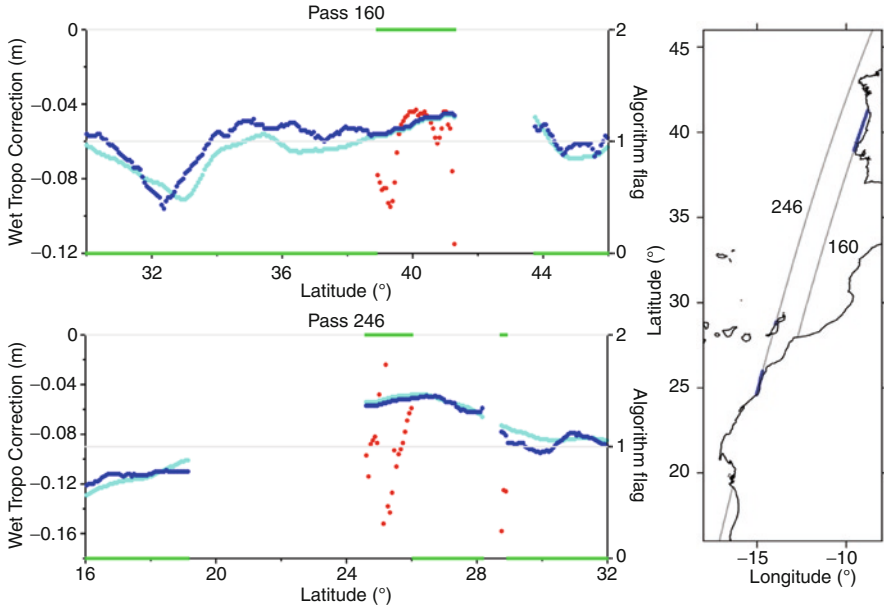
Fig. 6.1 Examples of the implementation of the DLM algorithm for two Envisat passes (Cycle 54). The top left figure shows path 160 crossing the Iberian Peninsula; the bottom left shows pass 246 crossing the Canary Islands and African coastline. The right plot illustrates the location of the passes

-8 ± 27 mm (difference between ECMWF and NCEP), reduces to -1 ± 7 mm after the DLM adjustment to the microwave radiometer field.

Being impossible to perform an accuracy assessment of the method using microwave radiometer measurements, this analysis gives an indication of the variability of the results when two different numerical weather models are used. This shows that ECMWF is more precise than NCEP and that the DLM adjustment to ECMWF will provide wet tropospheric corrections in the coastal region within an accuracy close to 1 cm.

6.2.2
GNSS-derived Path Delay Method

In recent years, an increasing number of inland GNSS (Global Navigation Satellite System) stations became available. In the scope of GPS (Global Positioning System) positioning, the tropospheric delay is often seen more as a nuisance factor, thus requiring effective estimation. Consequently, a vast number of developments have been pursued, aiming at the modelling of this effect (e.g., Hopfield 1971; Saastamoinen 1972; Niell 1996). GNSS data can be used to determine zenith tropospheric delays at the station location with an accuracy of a few millimetres (e.g., Niell et al. 2001; Snajdrova et al. 2006). The potential for the remote determination of atmospheric water vapour and integrated precipitable water also led to the development of several models mainly for meteorological purposes (e.g., Bevis et al. 1992). Within the scope of altimetry range correction, such data have been used with the purpose

of calibration of the wet tropospheric correction derived from the onboard microwave radiometers over offshore oil platforms (e.g., Bar-Sever et al. 1998; Edwards et al. 2004).

This section describes a method for deriving the wet tropospheric correction for coastal altimetry from GNSS-derived tropospheric delays, the so-called GPD (GNSS-derived Path Delay) approach. The method is based on tropospheric path delays (zenith hydrostatic delays, ZHD, and zenith wet delays, ZWD) precisely determined at a network of land-based or offshore GNSS stations, further combined with additional MWR measurements and data from a NWM, such as those produced by ECMWF. The following subsections describe the major issues and developments related to this approach. This is mainly based on work performed at the University of Porto (UPorto), Portugal, in the framework of the ESA-funded project COASTALT – Development of Radar Altimetry Data processing in the Oceanic Coastal Zone.

6.2.2.1
Determination of Tropospheric Path Delays at GNSS Stations

Methodologies for estimating the wet tropospheric delay from GNSS data are, at present, well-established and have been used by a vast number of authors; details can be found in Haines and Bar-Sever (1998), Desai and Haines (2004), Edwards et al. (2004) and Moore et al. (2005). A number of suitable software packages have been developed for the processing of GPS networks with the purpose of determining the tropospheric parameters, such as GAMIT (Herring et al. 2006), GIPSY/OASIS (Webb and Zumberge 1995) and Bernese (Dach et al. 2007).

Here, reference is given to the freeware GAMIT package (Herring et al. 2006), which is able to estimate a zenith path delay and its atmospheric gradient for each station, modelled in both cases by a piecewise-linear function over the span of the observations.

The tropospheric propagation delay is determined by GAMIT according to the following equation (Herring et al. 2006):

$$STD\,(E) = ZHD \times mf_h(E) + ZWD \times mf_w(E) \tag{6.1}$$

where STD is the slant total delay measured by GNSS, E is the elevation angle of the GNSS satellite and mf_h and mf_w are the mapping functions for hydrostatic and wet components, respectively.

A priori ZHD is evaluated from meteorological data using the modified Saastamoinen zenith hydrostatic delay model (Saastamoinen 1972; Davis et al. 1985) described by Eq. 6.8 (details in Sect. 6.4). In this way, for each slant total delay (STD) observation a combined zenith total delay (ZTD) is determined as the sum of ZHD and ZWD. At a given step interval (e.g., 1 h) and for each station of the defined network, a combined ZTD is estimated from the observations to all visible satellites.

For the determination of tropospheric parameters, a wide span of satellite elevation angles is advisable (Niell et al. 2001). For this reason, a relatively low (e.g., 7°) elevation cutoff angle can be adopted.

Since all stations belonging to the same regional network shall observe a given satellite with similar viewing angles, the corresponding zenith delays will be highly correlated. For

this reason, networks must include stations with a good global distribution in order to provide stability to the solution.

In the estimation procedure, mapping functions play a major role since they are responsible for the conversion between zenith and slant delays. The most commonly used mapping functions are all based on the same equation first proposed by Marini (1972): a continued fractions form in terms of sin(E) with coefficients a, b and c. What distinguishes the several mapping functions that have been used over the last decade are the values of the adopted coefficients, their derivation, and the knowledge of atmospheric composition and structure they express. Radiosonde data (Niell 1996), ray tracing through NWM (Niell 2001; Boehm and Schuh 2006) or climatologies (e.g., Boehm et al. 2006) have been used to derive the referred sets of coefficients.

The Vienna Mapping Functions 1 (VMF1, Boehm and Schuh 2004) are based on direct ray tracing through NWM. The VMF1 coefficients are derived from the pressure level data calculated by ECMWF and are given on a global $2.0° \times 2.5°$ latitude–longitude grid, four times a day, at 0, 6, 12 and 18 h UTC.

VMF1 are at present the mapping functions that allow a description of the atmosphere with the finest detail, leading to the highest precision in the derived tropospheric parameters. The climatology-based global mapping functions (GMF, Boehm et al. 2006) are used in GAMIT whenever VMF1 are not available.

In summary, the determined parameter is the combined ZTD. The separation of this quantity into a sum of ZHD and ZWD depends on the accuracy of the surface pressure data used to compute the ZHD component. The source of the hydrostatic corrections can be, for example, either the pressure values input to the model as *a priori* (every 6 h using VMF1 mapping functions) or measurements of station pressure recorded in a meteorological file, when available.

Comparisons made at four European stations (GAIA, CASCais and LAGos, in the coast of Portugal; MATEra in Italy), where ZHD values were computed from local surface pressure data and from VMF1 grids, show an agreement within 2–3 mm accuracy (1-σ). Therefore, the corresponding wet correction (ZWD) can be separated from the dry correction (ZHD) with the same accuracy.

The GNSS-derived tropospheric delays determined by GAMIT are quantities which refer to station location and therefore to station height. To be able to use these fields to correct altimeter measurements, the computed ZHD and ZWD have to be reduced to sea level by applying separate corrections for the two components. A procedure for computing the correction for station height is described in (Kouba 2008).

6.2.2.2
Comparison of GNSS-derived Tropospheric Fields with GDR Corrections

With the purpose of inspecting the suitability of GNSS-derived tropospheric parameters for correcting coastal altimetry, a comparison study between two types of tropospheric fields has been performed and is presented here. These fields are the GNSS-derived tropospheric corrections (dry or ZHD and wet or ZWD) at a network of European stations near the coast and the corresponding altimeter tropospheric corrections, usually present on GDR products, at the station's nearby points with valid radiometer correction.

The 3-year period of the analysis (July 2002 to June 2005) has been selected as the unique period for which there were four altimeter missions with different ground tracks:

TOPEX/Poseidon (T/P), Jason-1, Envisat and Geosat Follow-On (GFO). Altimeter data from these four missions have been used.

GNSS data were available for the same period, for a global network of about 55 IGS (International GNSS Service) and EPN (EUREF Permanent Network) stations. 30-s phase measurements were processed with the GAMIT software, using double differences and an elevation cutoff angle of 7°. IGS precise satellite orbits and clock parameters have been used (Dow et al. 2005).

Tropospheric parameters (ZHD + ZWD) were derived at 1-hour interval using VMF1 mapping functions and corrected for station height using the procedure described in (Kouba 2008). Although a shorter interval, e.g., 30 min, would be preferable, the 1-hour interval was adopted as a compromise between precision and computation time. The ZHD has been computed from *in situ* pressure data at each station (where available) or from the VMF1 grids, using the modified Saastamoinen model (Eq. 6.8 – Saastamoinen 1972; Davis et al. 1985). Tropospheric delays from a subset of 13 stations in the West European region (30° ≤ φ ≤ 55°, −20° ≤ λ ≤ 5°) have been selected for this study.

Altimeter tropospheric fields have been obtained from AVISO-corrected sea surface height (CorSSH, AVISO 2005). ZHD is the dry correction from ECMWF and ZWD is the wet microwave radiometer correction. Previous to any analysis, altimeter data have been stacked, i.e., interpolated into reference points along altimeter reference tracks.

For each point along each altimeter ground track, GNSS data of the surrounding stations have been interpolated for the altimeter measurement time. Therefore, for each altimeter point on the reference ground tracks, a set of time series of tropospheric fields have been generated: for the dry (ZHD) and wet (ZWD) altimeter tropospheric corrections and for the corresponding field determined at each GNSS station.

Various statistics have been computed for each pair of altimeter and station fields: correlation, mean and standard deviation (sigma) of the differences between the altimeter and the corresponding GNSS-derived field, for the station with maximum correlation. Results for the NW Iberia are shown on Fig. 6.2 and 6.3, for ZHD and ZWD, respectively.

Tables 6.1 and 6.2 show the statistics of the aforementioned fields represented in these figures, but for the whole study region (30° ≤ φ ≤ 55°, −20° ≤ λ ≤ 5°). Although points at larger distances have also been considered, in this statistical analysis only points up to 100 km distance of the GNSS station and at distances larger than 20 km from the coast have been included.

One of the first results that came out of this study was the importance of correctly performing the height corrections to the GNSS tropospheric fields, since the parameters determined at each station refer to station height and must be correctly reduced to sea level for use in satellite altimetry.

For ZHD, the height correction is almost a bias, a function of station height, and can reach several decimetres, as is the case of BELL station (h = 803 m) for which the mean correction reaches 0.212 m. For ZWD, the correction is smaller, a function of ZWD itself, and can reach several centimetres (mean correction is 0.043 m for BELL station).

The statistics presented show that the height correction is performed precisely by using the procedure in (Kouba 2008). For the comparison between GNSS-derived and Envisat ZHD, the statistics for the mean difference after correction are, in metres, −0.004, 0.004, −0.001 and 0.002 for minimum, maximum, mean and standard deviation, respectively. The corresponding statistics for ZWD are −0.013, 0.019, 0.002 and 0.007 (in metres). These values are a clear indication of the agreement between the altimeter and GNSS-derived fields.
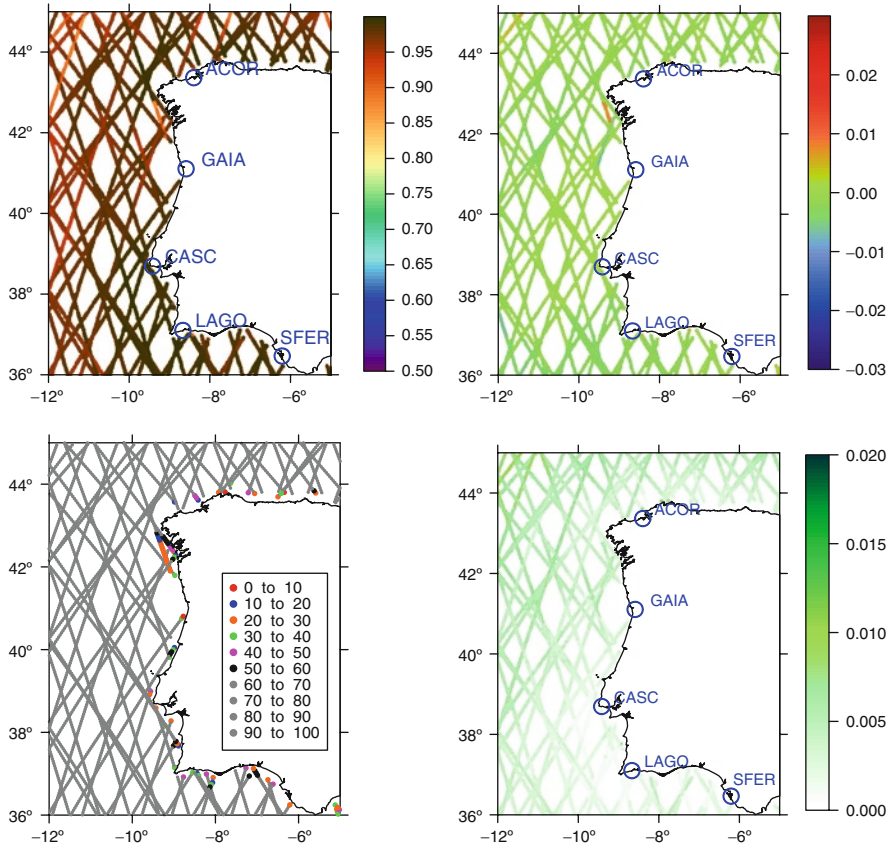
Fig. 6.2 Comparison between GDR ZHD at altimeter ground-track points and GNSS-derived ZHD at land-based stations. From *top* to *bottom* and *left* to *right* – for each ground-track point: maximum correlation, percentage of valid cycle points, mean and standard deviation of the differences between GDR ZHD and GNSS-derived ZHD (in metres) for the station with maximum correlation (x- and y-axis refer to longitude and latitude, respectively). Results refer to UPorto GNSS-derived solutions for period July 2002 to June 2005 and the NW Iberian region. GNSS-derived ZHD has been reduced to sea level

    As expected, results show that the distance to the station decreases the correlations increase (top left maps on Fig. 6.2 and 6.3) and the mean and sigma of the differences decrease in a consistent way (right maps on Fig. 6.2 and 6.3; top and bottom, respectively).

    The station showing maximum correlation with each altimeter track point is, in general, one of the closest stations, but not necessarily the closest one, because of local variations of the atmospheric fields, as shown in the bottom left map on Fig. 6.3.

    The bottom left map on Fig. 6.2, showing the percentage of valid cycle points for the study period, explains why for some close-to-land tracks the maximum correlation occurs for a station which is not in the vicinity of the point. In these cases, the time series have a small number of points and, therefore, the corresponding correlations are not statistically
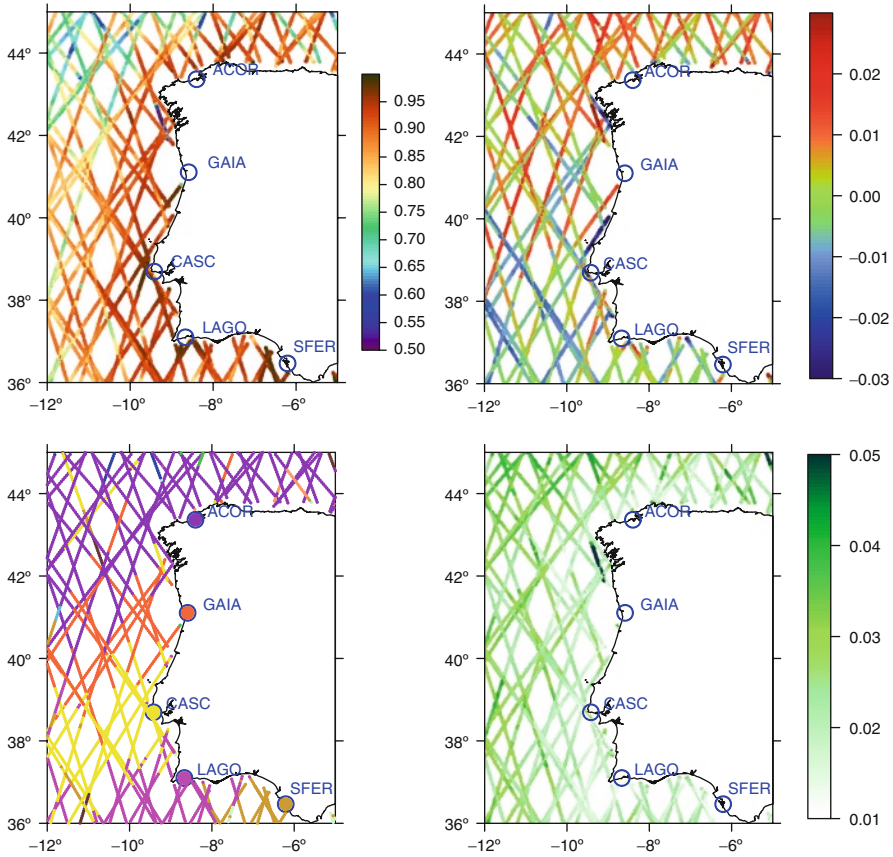
Fig. 6.3 Comparison between MWR-derived ZWD at altimeter ground-track points and GNSS-derived ZWD at land-based stations. From *top* to *bottom* and *left* to *right* – for each ground track-point: maximum correlation, GNSS station with which the correlation is maximum, mean and standard deviation of the differences between MWR- and GNSS-derived ZWD (in metres) for the station with maximum correlation (x- and y-axis refer to longitude and latitude, respectively). Results refer to UPorto GNSS-derived solutions for the period from July 2002 to June 2005 and the NW Iberian region. GNSS-derived ZWD has been reduced to sea level

significant. This is clear for the ascending 917 Envisat track almost parallel to the NW Spanish coast (percentage of valid cycle points below 30%).

When comparing the two fields (ZHD and ZWD), the highest correlations and the smallest differences are shown for ZHD since this field is easier to model and suffers the smallest variations; on the contrary, ZWD reveals the lowest correlations and the highest differences as it undergoes the largest spatial and temporal variations.

Overall, the results show that for distances up to 100 km the correlations are high (typically around 0.98 for ZHD and 0.93 for ZWD). For ZHD (Table 6.1), the mean difference is below 1 mm and the standard deviation of the differences has values around 2 mm for all missions. For ZWD (Table 6.2), although for all satellites the absolute mean difference is below 1 cm, actual values depend on the mission: around 2 mm for Envisat, 5 mm for

Table 6.1 Statistics for the comparison (altimetry-GPD) of sea level ZHD time series for altimetry track points (number in brackets) distant 20–100 km from maximum correlation GNSS station (difference and sigma in meters)

		Min	Max	Mean	Sigma
Envisat (461)	Difference	−0.004	0.004	−0.001	0.002
	Correlation	0.903	0.999	0.985	0.015
	Sigma	0.001	0.005	0.002	0.001
Jason-1 (157)	Difference	−0.002	0.004	0.000	0.002
	Correlation	0.944	0.997	0.986	0.012
	Sigma	0.001	0.004	0.003	0.001
T/P (120)	Difference	−0.003	0.005	0.000	0.002
	Correlation	0.967	0.997	0.985	0.008
	Sigma	0.001	0.005	0.003	0.001
GFO (298)	Difference	−0.003	0.004	0.000	0.002
	Correlation	0.846	0.996	0.977	0.036
	Sigma	0.001	0.008	0.003	0.001

Jason-1, −9 mm for T/P and −5 mm for GFO. The standard deviation of the differences has values around 16 mm for all satellites, which is within the expected variability for this field.

The different values for the mean differences in the ZWD field, shown on Table 6.2, suggest that there may be small biases between the microwave radiometers of the various satellites, a fact which is not unexpected. It appears that AVISO uses different editing criteria, resulting in quite different data amounts near the coast for the various missions. While for Envisat, Jason-1 and GFO, points are found down to the vicinity of the coast, for T/P the minimum distance is around 30 km. To mitigate this effect, only points at distances from the coast larger than 20 km have been considered. It should be highlighted that a precise comparison between the various missions solely based on the comparison with the GNSS data is difficult to achieve.

This study shows the suitability of the GNSS-derived tropospheric fields for use in the correction of the coastal altimeter measurements. However, owing to the relatively scarce number of GNSS stations, these fields have to be combined with additional available data to obtain the required spatial information.

As far as the tropospheric correction for coastal altimetry is concerned, providing GNSS-derived total correction (ZTD) seems to be as appropriate as providing the wet correction (ZWD) alone, since the dry or hydrostatic component (ZHD) is independently derived with very high precision.

6.2.2.3
Data Combination Methodology

An innovative approach to generate wet delay (ZWD) reliable estimates at satellite ground-track positions with invalid radiometer corrections (land-flagged) is by using a linear

Table 6.2 The same as Table 6.1 for ZWD

		Min	Max	Mean	Sigma
Envisat (595)	Difference	−0.013	0.019	0.002	0.007
	Correlation	0.766	0.999	0.933	0.039
	Sigma	0.005	0.029	0.016	0.004
Jason-1 (181)	Difference	−0.012	0.027	0.005	0.007
	Correlation	0.819	0.976	0.933	0.038
	Sigma	0.010	0.029	0.016	0.005
T/P (146)	Difference	−0.024	0.002	−0.009	0.006
	Correlation	0.835	0.982	0.946	0.027
	Sigma	0.008	0.028	0.015	0.004
GFO (326)	Difference	−0.017	0.008	−0.005	0.006
	Correlation	0.792	0.988	0.926	0.040
	Sigma	0.008	0.034	0.018	0.005

space-time objective analysis technique (Bretherton et al. 1976). The technique combines the available independent ZWD values derived from ECMWF model atmospheric fields with those from GNSS stations and with the microwave radiometer measurements (only those with valid MWR flag) to update a first guess value known *a priori* at each altimeter ground-track location with invalid MWR measurements. The statistical technique interpolates the wet correction measurements at the latter locations and epochs from the nearby (in space and time) MWR-, ECMWF- and GNSS-derived independent measurements, which are selected by imposing a data selection criterion, takes into account the respective accuracy of each data set, and updates the first guess value providing simultaneously a quantification of the interpolation errors. Therefore, the selected independent observations are weighted according to statistical information regarding their accuracy.

The combination of ZWD, rather than ZTD, independent quantities is preferred, since, as described before, the dry (hydrostatic component, ZHD) can be accurately derived from independent sources.

Besides the white noise associated with the measurements of each data set, the objective analysis technique requires *a priori* information on the ZWD signal variability and knowledge of the space-time analytical function that approximates the empirical covariance estimate.

Given these parameters, the generated estimates are optimal and no other accurate linear combinations of the observations, based on a least squares criterion, exist (Bretherton et al. 1976).

Spatial covariances between each pair of observations (valid MWR-, GNSS- or ECMWF-derived ZWD) and each observation and the location at which an estimate is required can be derived from a Gauss–Markov function (Schüler 2001), provided that the spatial correlation scale is known. Bosser et al. (2007) state that the ZWD varies spatially

and temporally with typical scales of 1 to 100 km and 1 to 100 min, respectively, and these ranges allow a preliminary establishment of the spatial and temporal correlation scales. In the results shown here, both the temporal and spatial correlation scales are assumed to remain constant over the analysed region ($30°N \leq \varphi \leq 55°N$, $20W° \leq \lambda \leq 20°E$). More accurate values are expected by fitting the empirical auto-covariance function.

In the absence of the knowledge of an empirical covariance model of the background field, covariance functions that decrease exponentially with the square of the distance (or time) between acquisitions can be adopted, although other analytical functions to model the observed covariance should be exploited.

The space variability of the ZWD field may be expressed by

$$F(r) = e^{-\frac{r^2}{C^2}} \tag{6.2}$$

where r is the distance between each pair of points and C is the spatial correlation scale. The temporal variability of the field is also taken into account by a stationary Gaussian decay (Leeuwenburgh 2000):

$$D(\Delta t) = e^{-\frac{\Delta t^2}{T^2}} \tag{6.3}$$

where Δt is the time interval between the acquisition of the measurements associated with each pair of locations and T is the temporal correlation scale. The covariance function is represented by the space-time analytical function $G(r, \Delta t)$ that is obtained by multiplying the space correlation function F(r) by the time correlation function $D(\Delta t)$.

The covariance matrix between all the pairs of observations and the covariance vector between observations and the location and epoch at which an estimation is required can be computed from $G(r, \Delta t)$ to within the signal variance. The function G is normalized so that the correlation equals unity when $r = 0$ and $\Delta t = 0$.

In the absence of sufficient data to perform the objective analysis, the algorithm gives the average value of the field calculated using the selected observations.

An example of implementation of this methodology is presented for Envisat cycle 58 (7 May 2007 to 11 June 2007) for the aforementioned geographical region. A MWR measurement has been considered invalid whenever its GDR land-ocean flag is set to 1 (land-flagged) or its quality interpolation flag is larger than 0 (the most comprehensive case). For these measurements, an estimation of the wet delay with an associated formal error is given by the implemented mapping routine. The observations include: valid MWR measurements acquired along the altimeter ground track, ZWD from GNSS land-based coastal stations (derived hourly and interpolated to a 30-min interval, further reduced to sea level) and ECMWF model-derived wet delay estimates (provided every 6 h at a regular 0.25° grid spacing). The latter were determined from two single-level parameter fields of the ECMWF deterministic atmospheric model: integrated water vapour (total column water vapour, TCWV) and surface temperature (2-m temperature, 2T) (ECMWF 2009). The formulation presented by Askne and Nordius (1987) was followed for the estimation of ZWD from TCWV, in which the mean temperature of the troposphere was modelled from 2T according to Mendes et al. (2000).

For the implementation of the objective analysis, the time and space correlation scales were set to 100 min and 100 km, respectively, and assumed constant over the whole period and study region. MWR-and GNSS-derived observations were assumed to have the same white measurement noise of 5 mm, while a value of 1 cm was assigned to white noise of the ECMWF-derived estimates. Since the observations have quite different spatial and temporal samplings, some issues must be addressed in the data selection criteria for the establishment of the influence domains to be considered in the merging procedures. The space domain radius was set equal to the space correlation scale, but given the temporal sampling of the ECMWF model, the temporal influence interval has been set to 3 h to guarantee that, at least, one model sample grid contributes to the estimation of the background wet delay field.

For each invalid MWR measurement, a first guess value has been computed as the mean value of the selected observations. The objective analysis procedure updates this value with the information added by the measurements themselves. The white noise of each data set and the data selection criteria were set as described above.

In order to compute the noise-to-signal ratio to set up the covariance matrix, the *a priori* knowledge of the signal variability is required. The *a priori* ZWD variability was computed using the data combination methodology and data from the three independent sources for the year 2007.

Using the information on the variability of the ZWD field, the data combination methodology generates a ZWD estimate along with a realistic relative mapping error value for the locations where the MWR measurements have been considered as invalid.

A more detailed analysis, not presented here, was performed for some Envisat passes very close to the Portuguese coast – passes 1, 74, 160, 917 – and allows a more elaborated discussion on the performance of the method. In general, the results show that when GNSS-derived wet delay values and valid MWR measurements are included in the selected observations, the wet delay estimates that result from the application of the methodology are clearly influenced by them. Output values show clear departures from the ECMWF values present in the GDR product. However, in most of the analysed cases, the variability of the field depicted by the ECMWF-derived values remains unchanged, i.e., when the ECMWF-derived values increase or decrease with time, the output field shows the same tendency. Moreover, results show that there are no significant biases between the computed wet delay values and the immediately adjacent valid MWR measurements. The continuity of the wet delay values is considered to be an added value of the implemented methodology.

Fig. 6.4 shows that the accuracy of the final GPD product is highly dependent on the availability and distribution of the three data sets used, in both time and space. In the worst case, the estimation is solely based on NWM measurements. Concerning the accessibility of present NWM, the ECMWF temporal sampling of 6 h is far from ideal, the required sampling being at least 3 h. Concerning the availability of valid MWR measurements, the worst cases take place when: (i) an isolated segment with all points with invalid radiometer measurements occurs; (ii) the track is parallel to the coastline, where a contaminated segment of several hundreds of kilometers length may occur. When the track is almost perpendicular to the coast there will be valid MWR measurements usually within a distance of 30–100 km. Considering the GNSS-derived path delays, various regions can be identified, particularly around European and USA coastlines, where relatively dense networks of coastal stations can be found. However, there are many regions without known available
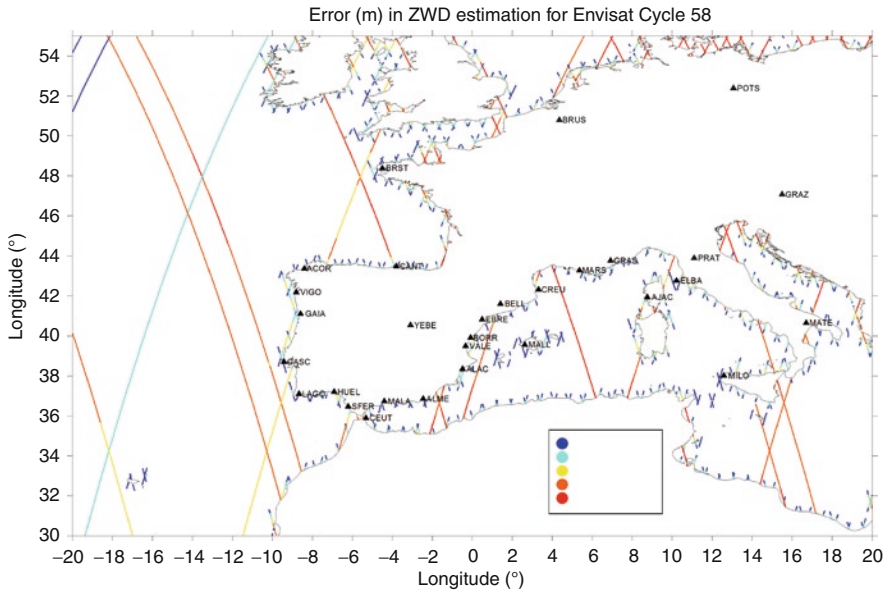
Fig. 6.4 Formal error (in metres) associated with the ZWD estimates calculated, using the datacombination methodology, for all invalid MWR measurements present in Envisat Cycle 58

GNSS stations for distances of several hundreds of kilometers. For this purpose, a densification of the network of coastal GNSS stations is advisable, with a station approximately every 100 km, preferably with meteorological sensors. Emphasis should be given to the merging of data derived from offshore GNSS stations (e.g., buoys and oil platforms) and local/regional NWM, whenever available.

6.3
Brightness Temperature Contamination and Correction

The algorithms used to retrieve the wet path delay from the measured brightness temperatures (TBs) implicitly assume that the satellite is flying over an oceanic surface. This is why the nominal retrieval method is unsuitable as soon as the satellite approaches the coasts, where the footprint contains land. The signal coming from the land surface is thus considered a "contamination". The study of this section is based on the following idea: if we know how to simulate this contamination, then we can remove it from the TBs to obtain a "clean" signal, i.e., without land-relative signal. From these corrected brightness temperatures, "decontaminated" measurements, we could then use the same oceanic retrieval everywhere, up to the coast.

To solve this problem, different methods have been proposed so far: Ruf proposed (Ruf 1999) an analytical and theoretical correction of TBs before retrieval. He assumed a track

perpendicular to a straight coastline. Bennartz (1999) tackled the problem of mixed land/water measurements ("footprints") in SSM/I data by taking the fraction of water surface within each footprint.

In this section, the TB contamination by land is analyzed in details and two correction methods are presented and evaluated.

6.3.1
Instrumental Configuration and Reference Field

Sensitivity studies are performed in TOPEX microwave radiometer (TMR) configuration, but the proposed methodologies are not dedicated to TOPEX; they are applicable to any other similar instruments onboard altimetry missions. The TMR operates at 18, 21 and 37 GHz with a footprint diameter of 44.6, 37.4 and 23.5 km, respectively (Ruf et al. 1995). The first TB is mainly sensitive to the surface roughness, the second to atmospheric humidity and the third to cloud liquid water (but all receive a significant contribution from the surface and atmosphere). TBs are available every second (which means about 7 km along track between two measurements).

It is almost impossible to provide a reliable evaluation of the proposed correction methods with real measurements, because of the spare availability of reference information available globally. To quantitatively evaluate the new methods, we therefore decided to use simulated brightness temperatures over reference meteorological fields with related instrumental characteristics. This way, it becomes possible to (i) characterize TBs' contamination by land when the satellite approaches the coasts, and (ii) evaluate quantitatively the performances of the different algorithms.

Details about the simulator development and its evaluation can be found in (Desportes et al. 2007). To sum up briefly, TBs are simulated with a radiative transfer model; over sea, the surface emissivity is derived from sea surface wind speed and sea surface temperature over land, monthly mean emissivity atlases are used, provided by Karbou et al. (2005). After computing local TBs (on each grid point), the map is then smoothed by a Gaussian function to simulate the antenna lobe, using the main lobe width that is function of the frequency. With this tool, we simulate the TBs that would have been measured by the TMR on each point of the grid (0.1° per 0.1°). Meteorological analyses are provided by the ALADIN model (see Hauser et al. 2003), the operational mesoscale forecast model of Météo-France. Surface fields of pressure, temperature, wind, as well as temperature and humidity profiles on 15 pressure levels are available at a 0.1° spatial resolution. The ALADIN meteorological analyses are used as geophysical reference fields. Two different cases were selected for this study: 16 March and 15 April 1998 because the ALADIN area was overpassed by TOPEX on the same track but in different atmospheric conditions. The first day corresponds to an off-shore dry wind, whereas for the second day of study, the atmosphere moisture over Mediterranean Sea is higher. The chosen track, number 187 (see Fig. 6.5), presents various interesting cases of contamination: clear land/sea and sea/land transitions (Algerian and French coasts), overflight of an island (Ibiza in the Balearic Islands), and track tangent to the coastline (Creus Cape in Spain).
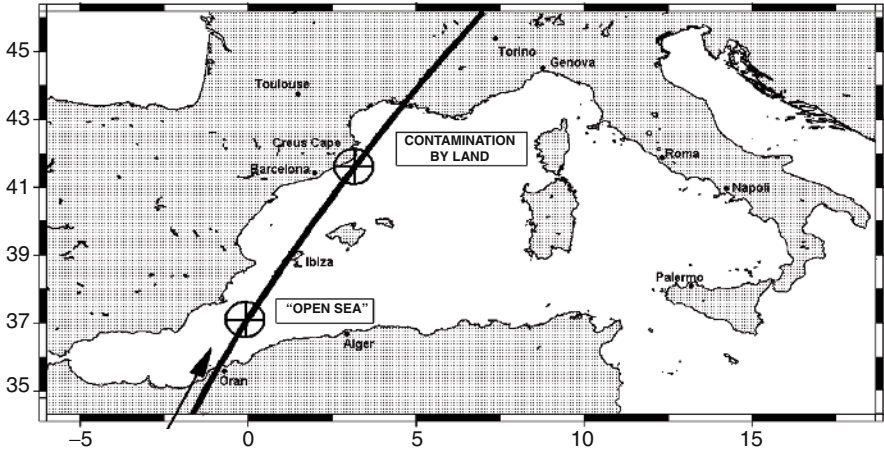
Fig. 6.5 TOPEX track number 187, 16 March around 12:00 (cycle 202) or 15 April around 06:00 (cycle 205)

6.3.2
An Analytical Correction of TBs: The "erf Method"

Ruf (1999) proposed an analytical correction of the measured TBs, function of the TB difference between sea and land. The track is assumed to be perpendicular to a straight coastline. TBs over sea and land are assumed to be constant. The major limitation of this method is the assumption that the track is perpendicular to the coastline. We propose, in the following, an improvement of the method by taking into account the angle between the track and the coast. Then, we test the sensitivity of this method.

6.3.2.1
Improved Method

Ruf used TBland and TBsea (taken 200 km after and before the transition) and a table of coefficients calculated for a track perpendicular to the coast, to calculate the following correction for a frequency ν and the distance d to the coast:

$$\text{corr}(d,\nu) = [\text{TBland}(\nu) - \text{TBsea}(\nu)] \times \text{table}(d,\nu) \tag{6.4}$$

First, we replaced the coefficients table by an erf function, primitive of a Gaussian function, which was found to fit well the actual sea-land TB evolution. The new correction is the following function:

$$\text{corr}(d,\nu) = \frac{\text{TBland}(\nu) - \text{TBsea}(\nu)}{2} \times \left(1 + erf\left(\frac{d}{\alpha(\nu,\theta)}\right)\right) \tag{6.5}$$

where d is the distance to the coast and α is a parameter conditioning the curve's slope at $d = 0$ (α only depends on the frequency ν and on the angle θ between the track and the coast). Fig. 6.6b shows the simulated TBs along an arbitrary track (Fig. 6.6a). The more the track is perpendicular to the coast, the shorter is the contamination by land. Simulated TBs are corrected using this function before applying the path delay (PD) retrieval algorithm. Whereas the PD error for uncorrected TBs on sea reaches values far greater than 1 cm (our reference), PDs from corrected TBs are obviously almost perfect, as we assumed perfectly known TBsea, TBland and θ.
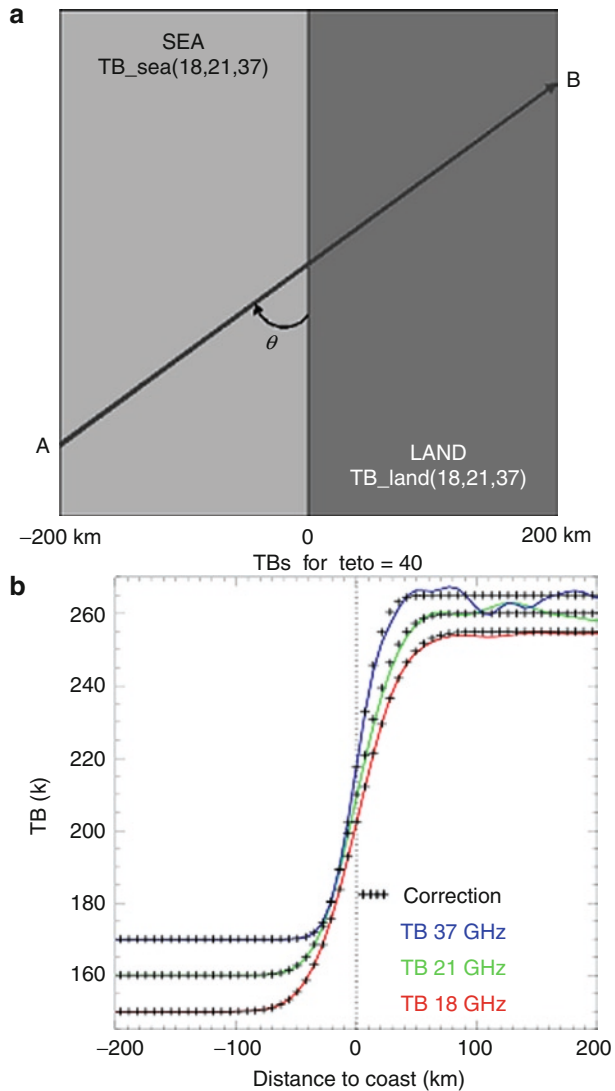

Fig. 6.6 (**a**) *Top*. Created track. The satellite goes from sea to land, crossing the coastline with a given angle; (**b**) *Bottom*. Simulated TBs along the created track presented above, from sea to land. A random noise is added to the simulated TBs over land, while the correction is unchanged

6.3.2.2
Sensitivity to Errors in θ or in TBland and TBsea

To evaluate the method in realistic conditions, we introduced different error types in TBland for simulated TBs, without altering the correction. We could have introduced this error on TBsea but TBs over land are more variable in space than over sea, and anyway the problem, as the correction function, is fully symmetrical.

By introducing a strictly equal bias on each frequency, we can accept a bias in TBland up to ±20 K to reach a 1-cm error on PD after correction. This can be explained by a compensation effect on the three channels. On the other hand, if we introduce an error only in one channel, assuming that TBland at the two other frequencies are perfectly known, the acceptable error bias is reduced to ±3 K to reach the limit of 1 cm. In other words, a relative error of 3 K is as damaging as a systematic bias of 20 K.

To generalize the error analysis, we introduced a Gaussian random error on TBland, independently on each channel, on one thousand samples. The maximum acceptable standard deviation on TBland is 2.7 K, to reach a mean error lower or equal to 1 cm on PD after correction (Table 6.3).

Finally, we introduced a random error on θ. The same error on θ will have a greater impact on PD if θ is small. For a θ value of 60°, a 40° error in θ estimation is allowed (to reach the limit of 1-cm error on PD). For a θ value of 20°, it decreases to 7°.

The land simulation case of the last line in Table 6.3 is the closest to reality: we estimated on the northwestern Mediterranean coast that the standard deviation of TBland is about 2.5 K for a 50-km segment coast. Fifty kilometers is the length of contamination for an angle between track and coast of about 25° at 18 GHz (or less in higher frequencies). This corresponds, therefore, to a mean error on PD of about 1 cm, which is already our limit. To this error, we have to add the one due to θ estimation and the one due to TBsea estimation. A θ angle of about 25° and a standard deviation of error on θ of about 10° lead to the limit of a 1-cm error on PD. If we estimate the error due to TBsea estimation to be 1 cm, the total error is about 1.7 cm. This is too much considering that the coast will never be actually rectilinear.

This method thus appears too sensitive to the geometry. Furthermore, it does not allow us to process complex cases like tangent tracks (what is θ in this case?) or islands (it is difficult to estimate θ and impossible to estimate TBland) or even small angles between track and coast. The complex pattern of the contaminating coast is not taken into account. As a consequence, this algorithm seems not adapted to a global operational processing.

Table 6.3 Error on PD after correction, when a Gaussian error is introduced on TBland

TBland standard deviation (K)	Mean error on PD after correction, on sea (cm)
20	6.5
10	3.5
5	1.6
2.7	1
2.5	0.8

6.3.3
Using the Proportion of Land in the Footprint

6.3.3.1
Description of the Proportion Method

This second approach is similar to (Bennartz 1999) in which Bennartz tackled the problem of mixed land/water measurements in SSM/I data by deriving the fraction of land surface within each measurement from a high-resolution land-sea mask. In this section, we describe the method we used to correct the TBs.

The correction function uses p, the actual proportion of land in the footprint. Far from coasts, p is zero on sea and 1 on land. The proportion p is calculated by means of a 0.01° resolution land-sea mask, taking into account the radiometer field of view characteristics. Therefore, p depends on frequency: at high frequencies the footprint is smaller. That is why, in the case of the island on track 187 (see Fig. 6.7a, first spike), contamination is greater at high frequencies. On the contrary, in the case of the tangent track, the smallest footprint hardly reaches the coast: it contains less land and the contamination is lower.

TBland and TBsea are estimated along the satellite track. For a complete sea-land transition, TBsea is the last uncontaminated TB (the last encountered TB with p = 0), and TBland is the first uncontaminated TB (p = 1). For incomplete transitions, we take the closest encountered TB (always along track) with p = 0 or 1.

This leads to the following correction function:

$$\mathrm{corr}(p,\nu) = [\mathrm{TBland}\,(\nu) - \mathrm{TBsea}\,(\nu)] \times p(\nu). \tag{6.6}$$

A comparison between simulated and measured TBs is shown in Fig. 6.7b. TBs are satisfactorily simulated near coasts: the simulated TBs obtained by adding the land contribution to the TBsea values fit well the real measurements performed by the TMR, even in the most complex configurations.
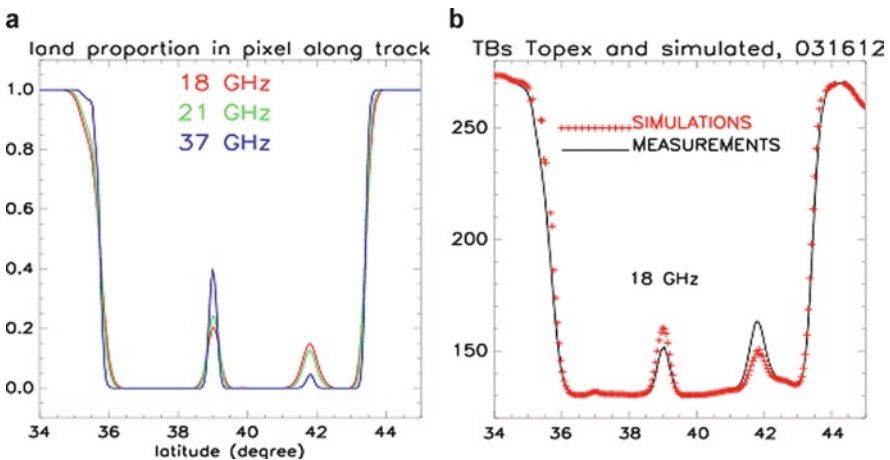

Fig. 6.7 (**a**) *Left*. Land proportion in the footprint along the track; (**b**) *right*. Simulations compared to actual measurements on the same track

6.3.3.2
Performance of the Method over Simulated Data

To test this correction on a large number of data, we simulate TBs along real TOPEX tracks. As the horizontal spacing of TOPEX tracks is very wide (about one track every 230 km), we add translated tracks to increase the horizontal resolution and number of cases.

We then apply the TB correction algorithm on each track, calculate the corrected PD and compare it, over sea with PDref. The PD obtained from contaminated TBs and the PD obtained propagating the last uncontaminated PD are also compared to PDref. In order to characterize the error in the coastal strip between the different obtained PDs and the ALADIN PD, we calculate the rms error for each transition case (262 cases among sea-land, land-sea, flying over an island or near a coast). Then, we calculate the quadratic mean of these rms errors. In this way, no case is favored: every transition has the same influence, whatever its length (if the angle between the track and the coast is small, the transition is longer).

Results are given in Table 6.4. The error near coasts is significantly reduced. We assume a linear dependency between the land proportion and the observed TBs. Nevertheless, this assumption is not always valid especially at 37 GHz, because of nonlinearity of the atmospheric radiative transfer for atmosphere-sensitive channels. Discrepancies with respect to the mean linear dependency come from atmospheric humidity variations above the surface (which is the signal we want to catch) but also from emissivity variations over sea and over land along the track (that are neglected in the proportion method).

This method is quite sensitive to the choice of TBsea and TBland, especially when the satellite overpasses an island. If the nearest point over land where $p = 1$ can be found at less than 200 km (in view of the characteristic atmospheric structures dimensions) the corresponding TBland value is assumed to be similar.

6.3.4
Performance Analysis over Real Measurements

By applying the retrieval algorithm to measured TBs without any correction, we calculate a "contaminated path delay". Then, using either the erf method (Sect. 6.3.2) or the proportion method (Sect. 6.3.3), we calculate two different "corrected path delays". The three

Table 6.4 RMS errors on the coastal strip between contaminated PD (initial PDsim)/propagated PDsim/corrected PDsim and PDref

	Contaminated PD (cm)	Propagated PD (cm)	Corrected PD (cm)
16 March	12.4	5.2	2.3
15 April	10.9	4.6	2.6

obtained PDs are compared with our reference, the ALADIN PD. We can benefit from the wide set of coastal transitions encountered within the ALADIN area to statistically evaluate the performances of the two methods.

Results are shown for the two different cases in Fig. 6.8. The obtained variations around coasts are consistent with the previous comparison. The signal near coasts is better corrected than over the island and tangent track cases. Again, the reason is the use of a distant TB. This appears as the major limitation of the method, since there is no way to estimate the adequate TB to use when there is no pure land footprint available.

Note that ALADIN PD cannot be used as a reference here, because of its negative bias with respect to TMR, and to its too smooth variations, compared with the actual ones.
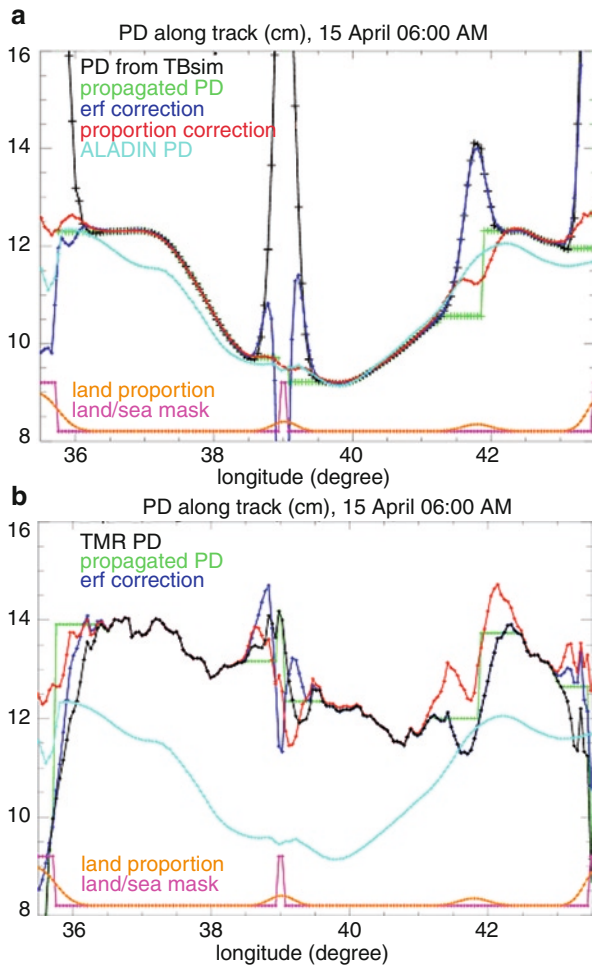

Fig. 6.8 Comparison between the PDs obtained from TBs after the different correction methods for track 187. (**a**) *Top*. Simulated TBs, (**b**) *Bottom*. Measured TBs

6.3.5
Discussion

The objective of this study was to analyze in detail the contamination of the brightness temperatures by land, and to propose a new approach. The validation of the different methods we have tested in this study is almost impossible using real brightness temperatures. We do not have enough in situ measurements (radiosondes, GPS) in coastal areas and no accurate enough model to fully evaluate the proposed corrections. We, therefore, chose to develop and use a simulator to perform sensitivity tests and to quantitatively evaluate the different methods for a large number of geometric and meteorological situations.

We first suggested refinements to the approach proposed by Ruf (analytical correction) (Ruf 1999). The results are satisfactory in a very optimal case (reduction by more than 60% of the error with respect to no correction). But sensitivity tests showed that the brightness temperature over land and the angle between the satellite track and the coast should be known with very good accuracy. However, these parameters are difficult to estimate, especially in complex geometries. Therefore, this method seems difficult to use globally in an operational processing.

The approach proposed by Bennartz (1999), developed for SSM/I mixed land-water footprints, has been adapted to the TOPEX/TMR case. It mainly uses the proportion of land in the footprint. This method is robust and seems more apt, because it allows the processing of any configuration. Results obtained on simulations are satisfactory, the error is 50% lower than with the previous method. But the hypothesis of a linear dependency between the land proportion and the observed TBs, not completely valid, leads to ignore atmospheric variations in the transition area. An additional limitation is the lack of information on TBland in the case of islands and tangent tracks (as in the previous method).

In this study, we used measurements from the TMR, collocated with the TOPEX/Poseidon altimeter measurements. Nevertheless, the proposed methodology is applicable to other radiometers, just taking into account the corresponding instrumental characteristics (frequency, footprint size, incidence angle). This method of decontamination of the brightness temperature also improves the retrieval of other radiometer products like the atmospheric attenuation of the altimeter backscattering coefficients and the cloud liquid water content.

6.4
Dry Tropospheric Correction

The dry tropospheric correction (or Zenith Hydrostatic Delay, ZHD) is responsible for about 90% of the total path delay caused by the troposphere on the altimeter measurement of the two-way travel time from the satellite to the nadir sea level (e.g., Chelton et al. 2001). It varies slowly in space and time – typical scales of 100–1,000 km and 3–30 h, respectively (Bosser et al. 2007). In fact, according to Bevis et al. (1992), the use of the term "dry" to refer to the hydrostatic component of the troposphere is actually misleading since it omits the fact that the water vapour indeed slightly contributes to the hydrostatic path delay as well.

Although it is by far the largest range correction to be performed, with values ranging from around 2.25 to 2.35 m, the estimation of the dry tropospheric correction is accurately performed solely based on sea level pressure (980–1035 hPa) (Chelton et al. 2001). Smith and Weintraub (1953) developed a semiempirical expression for the evaluation of the refractivity of the non-dispersive dry troposphere, later improved by Thayer (1974) and Liebe (1985), by accounting for the small contribution (~1%) of water vapour to the total pressure (and the compressibility factor of air). On the basis of the above approach, the dry tropospheric range correction (in cm) has been routinely estimated as

$$\Delta R_{dry} \approx 222.74 \, P_0 \, / \, g_0(\varphi) \tag{6.7}$$

(e.g., Chelton et al. 2001), where P_0 is the sea level pressure (in hPa) and $g_0(\varphi)$ is the acceleration due to gravity (in cm/s^2) at latitude φ. Several authors (e.g., Hopfield 1971; Saastamoinen 1972) worked upon the model expressed by Eq. 6.7 to develop the most commonly used expressions in geodesy and radio astronomy. The model in Saastamoinen (1972) was later revisited by Davis et al. (1985), yielding the expression

$$\Delta R_{dry} = \frac{0.0022768 \, P_0}{1 - 0.00266 \cos(2\varphi) - 0.00028 \, h} \tag{6.8}$$

where h is the ellipsoidal altitude (in km) and all the other variables have been defined above.

Although the dry tropospheric correction is only moderately sensitive to errors in the surface pressure, a 5 hPa accuracy would be needed to secure a 1-cm accuracy (Chelton et al. 2001). As direct measurements of surface pressure are seldom available over open ocean, the dry tropospheric correction estimations have to rely on pressure values derived from numerical weather models (NWM) as those from ECMWF or NCEP.

At present, the use of the modified Saastamoinen model together with NWM sea level pressure (e.g., ECMWF global 0.25° × 0.25° grids generated every 6 h) results in an uncertainty of less than 1 cm in the dry tropospheric range correction (Chelton et al. 2001). Recent studies (e.g., Bosser et al. 2007) further refined the Saastamoinen model (Eq. 6.8) by using an updated global Earth gravity model and a global climatology for air density (instead of the standard atmosphere of the original formulation). From the latter, it is claimed that an accuracy of 0.1 mm can be achieved for the dry correction providing surface pressure measurements can be guaranteed within an uncertainty of 0.1 hPa (requiring the use of high-accuracy barometers during quiet meteorological conditions, which does not usually happen).

For coastal altimetry applications, no degradation of the accuracy for the dry tropospheric correction is expected, since land-ocean transition has not been referred to as specifically affecting the time or space scales of surface pressure variation. Nevertheless, some work could be addressed to inspect possible shear at the land/sea interface and effects of night/day mass transport. As the accuracy of the dry correction basically relies on that of the surface pressure, coastal altimetry would surely benefit from the vicinity of the overland meteorological stations network (usually denser on the more populated coastal areas) eventually providing surface pressure data with higher temporal and spatial resolution than that currently obtained from global NWM. Although these data are, in principle, already assimilated into global NWM, the use of local models with higher spatial and

temporal resolution (e.g., ALADIN from Météo France/ECMWF) should be tested for the computation of improved dry tropospheric correction.

Any improvement on the estimation of the dry tropospheric correction will also impact the quality of the wet correction as derived from GNSS measurements, as the latter is obtained by subtracting the hydrostatic component to the GNSS-derived total correction, as previously described in this chapter. A number of studies (e.g., Bai and Feng 2003; Hagemann et al. 2003; Wang et al. 2007) have been conducted to assess the accuracy of the NWM-derived surface pressure for overland GPS stations locations. A comparison of the accuracy of the NWM-derived surface pressure with that obtained by collocated synoptic measurements for a set of land-based GPS stations can be found in (Chelton et al. 2001). Differences up to 3 hPa were reported by the authors to frequently occur, varying with station location and time of the year (significantly larger deviations were also found for some locations). Those differences did not present a specific and easy to model space or time pattern. As, unfortunately, only a very limited number of GPS stations are equipped with meteorological sensors, (Bai and Feng 2003) also stressed the need for seeking alternative sources for surface meteorological data or the use of solutions, which bypass the need for such data, if one wants to take advantage of the existing GPS networks. Hagemann et al. (2003) refer to a less than 1 hPa mean bias between collocated surface pressure measurements and those horizontally and vertically interpolated from nearby (up to a 100 km distance) World Meteorological Organization (WMO) stations. Wang et al. (2007) also found good results when using spatially and temporally interpolated synoptic surface pressure values from the 3-hourly WMO stations measurements.

Comparisons between dry tropospheric correction values present in Envisat Geophysical Data Records (GDR) files (cycles 30 to 64 – September 2004 to December 2007) and those derived from *in situ* surface pressure data at three GPS stations (GAIA, CASC and LAGO, in the coast of Portugal) show differences with a mean value of 0.002 ± 0.003 m that range from -0.005 to 0.020 m. In this analysis, only points within 100 km from each station and 50 km from the coast have been considered. Although the extreme values occur at ground-track points closer than 10 km from the coast, there is no clear degradation pattern associated with their distance to land.

6.5
Conclusions and Perspectives

To get workable altimetry products in coastal areas, specific corrections are needed. In the case of the wet tropospheric correction, different studies have been conducted recently and the first results are encouraging. The use of external information to describe more accurately the atmospheric humidity in the coastal band should allow a significant improvement in the quality of the altimeter products. Radiometer product deficiencies in these transition areas can be overcome by the use of valid MWR measurements in the vicinity of the points, of GNSS measurements from nearby stations, of meteorological models assuming a dedicated processing, or of land information (surface emissivity and temperature) to correct the brightness temperatures.

The DLM is a simple method that only requires GDR data, with optional distance-to-land information, is mission-independent and can be used as a backup method whenever a more

precise one is not available. A global implementation to 28 Envisat cycles, using two different NWM (ECMWF and NCEP), shows that the method reduces the rms of the differences between the NWM corrections at the coastal land-contaminated points from 28 to 7 mm, suggesting that the DLM implementation with ECMWF will provide wet tropospheric corrections in the coastal band with an rms accuracy close to 1 cm. The method fails when there are no valid radiometer measurements close enough to perform the adjustment (at about 6% of the points). In this case, the output can be the original model correction, adequately flagged.

GPD is an approach based on the combination of GNSS-derived path delays, valid MWR measurements and NWM-based information. The GPD estimated corrections are a combined value of all available measurements within the specified spatial (100 km) and temporal (100 min) scales. Therefore, the result is highly dependent on the spatial and temporal distribution of the three data types used. The most critical cases occur for isolated segments containing only invalid MWR measurements (the closest valid MWR measurements are at distances longer than 100 km) or tracks almost parallel to the coastline, for which there are no GNSS stations within a distance of 100 km. In this case, the estimated values are solely based on NWM measurements, assumed less accurate. A considerable number of configurations can be found, which allow the estimation of the wet delays within 1cm error: points at distances < 50 km from a GNSS station, points for which there are valid MWR measurements within a distance < 50 km or passes with an associated measurement time very close to the time of the closest NWM grid. To achieve this accuracy everywhere, an augmentation of the GNSS networks is advisable, ensuring a coastal station approximately every 100 km and, more importantly, in the locations where isolated segments occur containing all MWR measurements invalid. Considering a global implementation of the method, the accessibility of NWM grids at a higher temporal sampling, ideally 1 h, is of crucial importance.

The correction of brightness temperatures using the land proportion has been developed and tested in TMR configuration. Results are satisfactory and an operational version of the algorithm has been proposed and implemented in the Pistach prototype (Mercier et al. 2008) dedicated to a specific processing of the Jason-2 mission for coastal areas and inland waters. The implementation is quite simple, if auxiliary tables containing the proportion of land along the satellite track are computed first. The decontamination method is powerful but requires instrumental characteristics and very good *a priori* knowledge of the overflown surfaces. Performances are difficult to assess quantitatively because no reference values are available so far. Nevertheless, this method provides a radiometer wet tropospheric correction everywhere in the coastal band, and the improvement with respect to other estimations based on NWP models is evident in cases of high atmospheric variability (which is often the case near the coast) and/or inaccuracies in NWM estimations (smooth or wrong trends).

In conclusion, depending on the GNSS network density, on the atmospheric variability, which may condition the meteorological model accuracy, and on the geography knowledge (accuracy of the proportion of land), one method can be better than another. In a near future, it will be necessary to provide for each altimeter ground-track point the estimated value by the different methods and a quality flag or the associated accuracy, so that the user can decide which is the most suitable method for his application.

In parallel to the proposition of these new processing strategies, it is a necessity to think about new instruments with a much better spatial resolution and, therefore, a much smaller contamination area. In this context, the potential of high-resolution radiometers (higher than 150 GHz) with a much better spatial resolution and a much smaller land impact is

obvious and should be considered for future altimetry missions. Moreover, the estimation of GNSS-derived path delays will benefit from the augmentation of the GNSS coastal stations preferably equipped with meteorological sensors.

The dry correction can be accurately computed from pressure measurements. The present accuracy of the ECMWF-model-derived correction fulfils the requirements for open ocean. Results presented in this chapter indicate that in the coastal region the precision of this correction is still well within the 1-cm accuracy.

References

Askne J, Nordius H (1987) Estimation of tropospheric delay for microwaves from surface weather data. Radio Sci 22:379–386

AVISO (2005) Archiving, validation and interpretation of satellite oceanographic data. AVISO DT-CorSSH data are http://www.aviso.oceanobs.com/index.php?id=1267. Accessed June 2008

Bai Z, Feng Y (2003) GPS water vapor estimation using interpolated surface meteorological data from Australian automatic weather stations. J Global Position Syst 2(2):83–89

Bar-Sever YE, Kroger PM, Borjesson JA (1998) Estimating horizontal gradients of tropospheric path delay with a single GPS receiver. J Geophys Res 103(B3):5019–5035

Bennartz R (1999) On the use of SSM/I measurements in coastal regions. J Atmos Ocean Technol 16:417–431

Bevis M, Businger S, Herring TA, Rocken C, Anthes RA, Ware RH (1992) GPS meteorology: remote sensing of atmospheric water vapor using the global positioning system. J Geophys Res 97(D14):15787–15801

Boehm J, Schuh H (2004) Vienna mapping functions in VLBI analyses. Geophys Res Lett 31(L01603). doi:10.1029/2003GL018984

Boehm J, Niell A, Tregoning P, Schuh H (2006) Global mapping functions (GMF): a new empirical mapping function based on numerical weather model data. Geophys Res Lett 33(L07304). doi:10.1029/2005GL025546

Bosser P, Bock O, Pelon J, Thom C (2007) An improved mean-gravity model for GPS hydrostatic delay calibration. IEEE Geosci Remote Sens Lett 4(1):3–7

Bretherton FP, Davis RE, Fandry CB (1976) A technique for objective analysis and design of oceanographic experiment applied to MODE-73. Deep-Sea Res 23:559–582

Chelton DB, Ries JC, Haines BJ, Fu LL, Callahan PS (2001) Satellite altimetry. In: Fu LL, Cazenave A (eds) Satellite altimetry and earth sciences. International Geophysics Series, vol 69. Academic, pp 1–131, ISBN: 0-12-269543-3

Dach R, Hugentobler U, Fridez P, Meindl M (eds) (2007) Bernese GPS software - version 5.0. Astronomical Institute, University of Bern

Davis JL, Herring TA, Shapiro II, Rogers AEE, Elgered G (1985) Geodesy by radio interferometry: effects of atmospheric modelling errors on estimates of baseline length. Radio Sci 20(6): 1593–1607

Desai SD, Haines BJ (2004) Monitoring measurements from the Jason-1 microwave radiometer and independent validation with GPS. Mar Geod 27(1):221–240. doi:10.1080/01490410490465337

Desportes C, Obligis E, Eymard L (2007) On the wet tropospheric correction for altimetry in coastal regions. IEEE Trans Geosci Remote Sensing 45(7):2139–2149

Dow JM, Neilan RE, Gendt G (2005) The international GPS service (IGS): celebrating the 10th anniversary and looking to the next decade. Adv Space Res 36 (3):320–326, 2005. doi:10.1016/j.asr.2005.05.125

ECMWF (2009) http://www.ecmwf.int/products/catalogue/pseta.html

Edwards S, Moore P, King M (2004) Assessment of the Jason-1 and TOPEX/Poseidon microwave radiometer performance using GPS from offshore sites in the North Sea. Mar Geod 27(3):717–727. doi:10.1080/01490410490883388

Fernandes MJ, Bastos L, Antunes M (2003) Coastal satellite altimetry – methods for data recovery and validation. In: Tziavo IN (ed) Proceedings of the 3rd meeting of the international gravity & geoid commission (GG2002), Editions ZITI, pp 302–307

Hagemann S, Bengtsson L, Gendt G (2003) On the determination of atmospheric water vapor from GPS measurements. J Geophys Res 108(D21):4678. doi:10.1029/2002JD003235

Haines BJ, Bar-Sever YE (1998) Monitoring the TOPEX microwave radiometer with GPS: stability of columnar water vapour measurements. Geophysic Res Lett 25(19):3563–3566

Hauser D et al. (2003) The FETCH experiment: an overview. J Geophys Res 108(C3):8053. doi:10.1029/2001JC001202

Herring T, King R, McClusky S (2006) GAMIT reference manual – GPS analysis at MIT – Release 10.3. Department of Earth, Atmospheric and Planetary Sciences, Massachusetts Institute of Technology

Hopfield HS (1971) Tropospheric effect on electromagnetic measured range: prediction from surface weather data. Radio Sci 6:357–367

Karbou F, Prigent C, Eymard L, Pardo JR (2005) Microwave land emissivity calculations using AMSU measurements. IEEE Trans Geosci Remote Sensing 43(5):948–959

Kouba J (2008) Implementation and testing of the gridded Vienna mapping function 1 (VMF1). J Geod 82:193–205. doi:10.1007/s00190-007-0170-0

Leeuwenburgh O (2000), Covariance modelling for merging of multi-sensor ocean surface data, methods and applications of inversion. In: Hansen PC, Jacobsen BH, Mosegaard H (eds) Lecture notes in earth sciences, vol 92. Springer, pp 203–216. doi:10.1007/BFb0010278 is Berlin/Heidelberg

Liebe HJ (1985) An updated model for milimeter wave propagation in moist air. Radio Sci 20(5):1069–1089

Marini JW (1972) Correction of satellite tracking data for an arbitrary tropospheric profile. Radio Sci 7(2):223–231

Mendes VB, Prates G, Santos L, Langley RB (2000) An Evaluation of the accuracy of models of the determination of the weighted mean temperature of the atmosphere. In: Proceedings of ION, 2000 national technical meeting, January 26–28, 2000, Pacific Hotel Disneyland, Anaheim, CA

Mercier F (2004) Amélioration de la correction de troposphère humide en zone côtière. Rapport Gocina, CLS-DOS-NT-04-086

Mercier F, Ablain M, Carrère L, Dibarboure G., Dufau C, Labroue S, Obligis E, Sicard P, Thibaut P, Commien L, Moreau T, Garcia G, Poisson JC, Rahmani A, Birol F, Bouffard J, Cazenave A, Crétaux JF, Gennero MC, Seyler F, Kosuth P, Bercher N (2008) A CNES initiative for improved altimeter products in coastal zone: PISTACH. http://www.aviso.oceanobs.com/fileadmin/documents/OSTST/2008/Mercier_PISTACH.pdf

Moore P, Edwards E, King M (2005) Radiometric path delay calibration of ERS-2 with application to altimetric range. In: Proceedings of the 2004 Envisat & ERS symposium, Salzburg, Austria 6–10 September 2004

Niell AE (1996) Global mapping functions for the atmosphere delay at radio wavelengths. J Geophys Res 101(B2):3277–3246

Niell AE (2001) Preliminary evaluation of atmospheric mapping functions based on numerical weather models. Phys Chem Earth 26:475–480

Niell AE, Coster AJ, Solheim FS, Mendes VB, Toor PC, Langley RB, Upham CA (2001) Comparison of measurements of atmospheric wet delay by radiosonde, water vapor radiometer, GPS, and VLBI. J Atmos Ocean Technol 18:830–850

Ruf C (1999) Jason microwave radiometer – land contamination of path delay retrieval. Technical note for the Jason project

Ruf C, Keihm S, Janssen MA (1995) TOPEX/Poseidon microwave radiometer (TMR): I. Instrument description and antenna temperature calibration. IEEE Trans Geosci Remote Sensing 33(1):125–137

Saastamoinen J (1972) Atmospheric correction for troposphere and stratosphere in radio ranging of satellites. In: Henriksen S, Mancini A, Chovitz B (eds) The use of artificial satellites for geodesy, vol 15. Geophysics Monograph Series, AGU, Washington, DC, pp 247–251

Scharroo R, Lillibridge JL, Smith WHF, Schrama EJO (2004) Cross-calibration and long-term monitoring of the microwave radiometers of ERS, TOPEX, GFO, Jason and Envisat. Mar Geod 27:279–297

Schüler T (2001) On ground-based gps tropospheric delay estimation. PhD thesis, Universität der Bundeswehr München, Studiengang Geodäsie und Geoinformation available at http://ub.unibw-muenchen.de/dissertationen/ediss/schueler-torben/inhalt.pdf. Accessed 13 January 2009

Smith EK, Weintraub S (1953) The constants in the equation for atmospheric refractive index at radio frequencies. Proc Inst Radio Eng 41(8):1035–1037

Snajdrova K, Boehm J, Willis P, Haas R, Schuh H (2006) Multi-technique comparison of tropospheric zenith delays derived during the CONT02 campaign. J Geod 79:613–623. doi:10.1007/s00190-005-0010-z

Thayer GD (1974) An improved equation for the radio refractive index of air. Radio Sci 9(10):803–807

Wang J, Zhang L, Dai A, Van Hove T, Van Baelen J (2007) A near-global, 2-hourly data set of atmospheric precipitable water from ground-based GPS measurements. J Geophys Res 112(D11107). doi:10.1029/2006JD007529

Webb FH, Zumberge JF (1995) An introduction to GIPSY/OASIS-II. JPL Publication D-11088, Jet Propulsion Laboratory, Pasadena